To be submitted to AJ; draft May 21, 2013

WISE J061135.13-041024.0AB: A J-Band Flux Reversal Binary at the L/T Transition

Christopher R. Gelino[1], et al.

ABSTRACT

We present Keck LGS-AO observations of WISEP J061135.13-041024.05 showing it is a binary with a component separation of 0.″4. This system is one of 7 in which the magnitude differences between the components show a reversal in sign between the J band and the H and Ks bands. Deconvolution of the composite spectrum results in a best fit binary solution with consisting of L9 and T1.5 components. We also present a preliminary parallax placing the system at a distance of 25pc.

Subject headings: stars: binaries: general — stars: fundamental parameters — stars: individual (WISEP J061135.13-041024.05;) — stars: low mass, brown dwarfs

1. Introduction

The H-band flux of stellar objects changes by nearly 12 orders of magnitudes from O stars down to the Y dwarfs (Kirkpatrick et al. 2012). The progression of absolute H magnitude (M_H) along this sequence is fairly smooth except for two major kinks. The first occurs in the early M dwarfs, where the formation of H_2 at these temperatures results in a short plateau in M_H (Mould 1976; Mould & Hyland 1976).

The other kink lies at the transition between the L and T dwarfs. It is here that the absolute H magnitude shows a slight increase to brighter magnitudes before turning downward at the early T dwarfs. This feature is even more pronounced in the J band, earning the label the "J-band bump" (Tinney et al. 2003). There are two dominant theories for the source of the bump.

[1]NASA Exoplanet Science Institute, California Institute of Technology, Pasadena, CA 91125, USA

One theory for the brightening is related to the clouds present in the atmospheres of these cool objects. The atmospheric models of L dwarfs require the presence of clouds in order to replicate the observed spectral and photometric trends. Conversely, models to match the observed properties of T dwarfs require the clouds to be completely dissipated, leaving the atmospheres clear of condensates. The transition from the cloudy L dwarfs to the clear T dwarfs is not well understood and has been notoriously difficult to model. A gradual lowering of a cloud deck through the L to T cooling sequence produces a shift in the near-IR magnitudes that is too slow to account for the observed colors and absolute magnitudes of L and T dwarfs (Knapp et al. 2004). However, Tsuji & Nakajima (2003) find that the transition can be modeled with a slowly dropping cloud deck if the objects populating the transition region have a large range of gravities. Specifically, the bright T dwarfs would have lower masses and gravities compared to the late L dwarfs.

An alternate theory is that the brightening is caused by the rapid evolution and clearing of the cloud layer (Burgasser et al. 2002; Knapp et al. 2004). Small holes in the cloud deck allows hotter flux from deeper in the atmosphere to emerge, resulting in a slightly brighter luminosity and bluer $J-K$ color. The clearings can also explain resurgence of FeH in the late-L to early T as the FeH in the hotter atmosphere below the clouds becomes visible(Burgasser et al. 2002).

A third prominent theory for the brightening is that the feature is caused by brown dwarfs having a spread of different gravities, effective temperatures, metallicities, and rotation rates (Burrows et al. 2006). Thus, the bump is not a single group of objects with a particular set of properties. Rather, the combination of brown dwarfs with wide-ranging characteristics disperses the absolute magnitudes into the observed, apparent brightening. To test this theory, it is necessary to derive the gravities, effective temperatures, metallicities, and rotation rates for objects in and around the bump. Unfortunately, these properties are very difficult to derive.

One thing that is certain, however, is that the brightening is an intrinsic property of the brown dwarfs and does not appear to be the result of any type of selection effect. Several binary systems (see Table 1) have been discovered in which the secondary is brighter than the primary in the 1-1.3μm region. These binaries typically consist of a late-L to early-T dwarf primary with a early-mid T dwarf secondary.

In this paper we present a 7th binary showing a flux reversal in the 1-1.3μm region. WISEP J061135.13-041024.05 (WISE 0611−0410, hereafter) was first presented in Kirkpatrick et al. (2011) as a T0 with a spectro-photometric distance of 17.7 pc. It was discovered in a search for bright sources from the Wide-field Infrared Survey Explorer (WISE; Wright et al. 2010) with brown dwarf-like colors, but with no counterpart in the 2MASS

catalog. Such properties are indicative of a source that either has a large proper motion or one with a very red $J - W2$ color. In the case of WISE 0611−0410 the source is present in the 2MASS catalog, but its position has moved by more than 3″ between the two surveys. Follow-up observations discussed here have more accurately measured the proper motion and provide a first determination of the parallax. We also show resolved photometry and spectral deconvolution that clearly demonstrate the flux reversal in the 1-1.3μm region.

2. Observations

2.1. NTT

The parallax observations were carried out using the ESO 3.5m New Technology Telescope and its infrared spectrograph and imaging camera SOFI (Moorwood et al. 1998) as part of program 186.C-0756: *NTT Parallaxes of Southern Extremely Cool objects* . The observing, analysis and reduction procedures are described in detail in Smart et al (2013) and here we will only briefly summarize them. The observations were made in SOFI's large field mode providing a field of view of 4.9′ x 4.9′ with 0.″288 pix^{-1} in the J band. We carried out 18 point dither observations with 4 iterations of 30 seconds at each point for a total exposure time of 36 minutes. The observations were combined using the *jitter* routine of the *Eclipse* (Devillard 1997) version 5.0 package. All objects in the field were found and centroided using the Cambridge Astrometry Survey Units *imcore* maximum likelihood barycenter software (CASUTOOLS, v 1.0.21).

During nights of exceptional seeing, our NTT observer, R. Mendez, noted that the PSF of WISE 0611−0410 was slightly elliptical compared to other objects in the field. This prompted the high-resolution follow-up and spectral analysis discussed here.

2.2. Keck II/NIRC2

High resolution images of WISE 0611−0410 were obtained using the Keck II LGS-AO system (Wizinowich et al. 2006; van Dam et al. 2006) with NIRC2 on the nights of 2012 Jan 13, 2012 Apr 15, 2012 Sep 06 & 2012 Nov 29 (see Table 3). Because our target was too faint in R-band to serve as a tip-tilt reference star for the wavefront corrector, we used the USNO-B star 0858-0074221 (Monet et al. 2003) with R=16.5 and located 35″ from our target. Our interest was only in the target and its immediate vicinity, so we used the narrow camera mode with a nominal pixel scale of 9.942 mas pix^{-1} and single-image field of view of 10″. We used a 3-point dither pattern to avoid the high noise levels in the lower-left quadrant

of the array. This pattern was repeated with different offsets to build up a longer exposure. The MKO H filter was used on all nights and the MKO J and K_s filters were used on only 2012 Apr 15.

The images were reduced using scripts in the IDL environment. A dark frame was first subtracted from each science frame. Then, a sky frame, created from the median average of all images acquired for WISE 0611−0410 exclusive of the frame being reduced, was subtracted. The sky-subtracted frames were then divided by a dome flat. Finally, the images were shifted to align the target to a common location and a deep mosaic was created from the median average of the stack. For the single image obtained on 2012 Nov 29, we could only dark subtract and flat-field the science frame. Fortunately, since our interest in that data was to follow the relative motions of the objects, the lack of a sky frame did not impede our goals.

The J, H, and K_s mosaics from 2012 Apr 15 are shown in Figure 1. As was suspected from the NTT data, this source is easily resolved into two components. Visual inspection of the images shows that the relative brightness changes sign between the J and H & K_s images. We discuss the implications of this below.

3. Analysis

3.1. Parallax and Proper Motion

We have 20 observations of WISE 0611−0410 started in 2010-12-23 through 2013-02-28. A observation in the middle was chosen as the master frame and the measured coordinates transformed to a standard system using the 2MASS objects in the field. All other observations were transformed to this standard system using all common objects and a simple linear transformation. Once all frames are on the same system the motion of the target was fit for the astrometric parameters: position, relative proper motion and relative parallax. This procedure was iterated and anonymous stars with high errors were removed and also one frame with a large residual compared to the best fit was also dropped. After this iteration a correction of the relative parallax to an absolute values was calculated using the galaxy model of Mendez and van Altena (1996). The resulting sky motion along with our fit is shown in figure 2 and the astrometric parameters are produced in table 4.

3.2. Resolved Photometry

As shown above, we were easily able to resolve WISE 0611−0410 into its component source and obtained magnitude differences in the MKO J, H, and K_s filters. H and K images of WISE 0611−0410 were obtained by UKIDSS. These images show an elliptical source, similar to what is seen in the NTT data. However, no J_{MKO} images of this field have been obtained. Therefore, we estimate the J_{MKO} magnitude based on the work of Stephens & Leggett (2004). First, we use the 2MASS J–spectral type relation in Table 4 of that paper to compute a J_{MKO} magnitude of 15.31±0.05. The second method, based only on the 2MASS J and K_s magnitudes as presented in Table 5 of Stephens & Leggett (2004), gives J_{MKO}=15.33±0.06. Given that these two methods are entirely consistent, we take the average of these two methods as the MKO J magnitude of WISE 0611−0410 and present it in Table 2.

The separation between the two components is large enough that simple aperture photometry can be used to measure the magnitude differences. We use the data from 15 April 2012 for the photometry since it is the highest quality and it includes the largest set of filters (J, H, and K_s). The photometry is performed on the mosaicked images (Figure 1) and is presented in Table 5.

The relative fluxes of the components show the same sign reversal from J to H and K_s as can be readily seen in the mosaic. This is one of only 6(?) such binary systems to show a flux reversal in the components: We denote the source that is fainter at J as component A in this system.

3.3. Resolved Astrometry and Companionship

We have observed WISE 0611−0410 using high-resolution imaging on 4 different epochs with the purposes of confirming a common proper motion between the sources and searching for any orbital motion. For a given epoch, we measure the separation in RA and Dec from source A to source B on all of the individual images. We then take the average separations from the measurements and assign the standard deviation as the error in those quantities. Since the 2012 Sep 06 epoch only contained a single, good quality image, we conservatively set the separation error in each axis to be 10 mas (≈1 pixel).

The final measurements are shown in Table 6 and graphically in Figure 7. If source B was a background object, then its position would have changed by 250 mas over the course of the NIRC2 observations. A positional offset that large is easily detectably in these high quality observations. However, there is no significant change in the relative position of

source B over the four epochs. Therefore, we can confidently confirm that these sources are physically bound and, additionally, not orbital motion is yet detected.

3.4. Composite Spectrum Deconvolution

To determine the spectral types of the individual components of WISE J061135.13−041024.0 we used a three-step deconvolution procedure, similar to that described in Day-Jones et al. (2013). First we fit the entire spectrum (0.85-2.45 μm) of our target with the near-infrared spectroscopic standards defined in Kirkpatrick et al. (2010) and Burgasser et al. (2006), determining the best-fit standard via χ^2 minimization. The best-fit standard selected this way is the T0 SDSS J120747.17+024424.8. This spectral type is consistent with the spectral type found by Kirkpatrick et al. (2011).

Then we repeated the fit using a set of synthetic binaries. Synthetic binaries were created combining the template spectra taken from the SpeX-Prism library[1], scaling them to the appropriate relative flux level using the spectral type−absolute magnitude calibration presented in Marocco et al. (2010). We selected only those binaries giving a lower χ^2 compared to the standard template. Finally, the best-fit binary was find among those by only fitting three regions of the spectrum: 1.1-1.25 μm (containing CH_4 and H_2O absorption bands), 1.55-1.75 μm (containing the CH_4 absorption band), and 2.1-2.35 μm (containing the CO absorption band). The features within these intervals change significantly at the transition between L and T types, and are therefore the most suitable to identify and deconvolve unresolved L/T pairs. The best-fit template identified with this procedure consists of a L9 (SDSS J085234.90+472035.0) and a T1.5 (SDSS J175024.01+422237.8).

We tested the significance of our deconvolution using an F-test to compare the result of the fit with synthetic binaries against the fit with the standard template alone. If the ratio of the two χ^2 (η) is larger than the critical value (η_{crit}) than the combined template provides a better fit at the 99.5% confidence level. We obtained $\eta = 1.73$ larger than the critical value $\eta_{crit} = 1.41$. We therefore assign spectral types of L9 and T1.5 for the two components.

3.5. Discussion

The resolved photometry and parallax measured here allow us to compare WISE 0611−0410 with other brown dwarfs. In Figures 3, 4, and 5, we use the absolute magnitudes and spectral

[1]http://pono.ucsd.edu/∼adam/browndwarfs/spexprism/

types estimated from the spectrum deconvolution to compare WISE 0611−0410 to other L and T dwarfs from Dupuy & Liu (2012) and Burgasser et al. (2013). Both components appear to be normal with respect to similarly-typed brown dwarfs. However, since both spectral types are determined from the deconvolution of the composite spectrum, they should only be regarded as estimates. The color-magnitude diagram shown in Figure 6 bypasses the spectral type uncertainty by making the comparison based entirely on the well-measured photometry and parallax. Again, there is nothing to suggest that this system has significantly different age, metallicity, or cloud coverage compared to most other brown dwarfs.

In order to estimate the orbital period of this system we first need to estimate the orbital semi-major axis and the masses of the components. SInce we have not detected any orbital motion of the secondary, we estimate the semi-major axis using the currently observed angular separation (0.″392) and distance (21.2 pc). The resultant projected separation (8.31 AU) is statistically likely to be smaller than the semi-major axis by a factor of 1.26 (Fischer & Marcy 1992). Thus, we estimate the semi-major axis to be 10.5 AU.

Obtaining estimates for the component masses requires several steps and assumptions. First, we use the K-band bolometric correction (BC_K)–spectral type relation from Looper et al. (2008) to compute BC_K, and in turn, the absolute bolometric magnitude (M_{bol}) for the components. M_{bol} for the primary and secondary are 16.26±0.17 and 16.63±0.17, respectively. Next, we use the absolute bolometric magnitudes to derive the luminosities of the objects with respect to the sun by the simple relation

$$M_{\mathrm{bol}} - M_{\mathrm{bol},\odot} = -2.5\log(\mathrm{L}/\mathrm{L}_\odot)$$

and the adoption of $M_{\mathrm{bol},\odot}$=4.61 (Cox 2000; Torres 2010). We find luminosities of 2.2×10^{-5} $\mathrm{L}_\odot$ and 1.6×10^{-5} $\mathrm{L}_\odot$ for the primary and secondary components, respectively.

The component masses are computed from Eqn. 1 from Burrows et al. (2001) using the assumption that the Rosseland mean opacity for these objects is 10^{-2} cm^2 gm^{-1}, effectively setting that term in the relation to 1. The other unknown in that relation is the age of the object, which is, unfortunately, often very difficult to infer. The composite spectrum does not show any indicators that this system is very young, so we assume that the age of the system is more than a few hundred million years old (Kirkpatrick 2005). For the purposes of this exercise, we use age values of 0.5, 1.0, 3.0, and 5.0 Gyr, typical of disk population stars (Reid & Hawley 2000). The resultant masses are shown in Table 7. Not surprisingly, the large range of ages produces a disperse set of masses, from 30-90 $\mathrm{M}_{\mathrm{Jup}}$ for the primary and 25-80 $\mathrm{M}_{\mathrm{Jup}}$ for the companion. Likewise, the orbital periods computed from these masses have a wide spread: 80-150 years. Unfortunately, the long periods mean that it will take decades of monitoring to really establish the true orbital period and component masses.

4. Conclusions

We have discovered a new brown dwarf binary system that straddles the L/T dwarf transition. Resolved, differential photometry shows that the earlier-type primary is *fainter* than the cooler secondary in the J band, but brighter in H and K_s, making this system one of 7 that shows a flux reversal in the 1-1.3 μmregion. Although we do not have resolved spectroscopy of the components, deconvolving the composite spectrum into two spectra indicates the best-fit spectral types are L9 and T1.5. We also present a new parallax of the system placing it at 21.1pc. Comparison to other L and T dwarfs shows that this system does not appear to have any unusual metallicity or age properties compared to the bulk of the field brown dwarfs, making it a good system to study for characterizing solivagant brown dwarfs. However, with an orbital period estimated to be >80 years, it will be some time before a good determination of the components masses can be made.

The authors acknowledge telescope operators Julie Rivera, Heather Hershley, and Gary Punawai, and instrument specialists Al Conrad, Marc Kassis, and Scott Dahm at Keck, for their assistance during the observations. Data presented herein were obtained at the W. M. Keck Observatory from telescope time allocated to the National Aeronautics and Space Administration through the agency's scientific partnership with the California Institute of Technology and the University of California. The authors recognize and acknowledge the very significant cultural role and reverence that the summit of Mauna Kea has always had within the indigenous Hawaiian community. We are most fortunate to have the opportunity to conduct observations from this mountain.

Facilities: Keck (NIRC2,LGS)

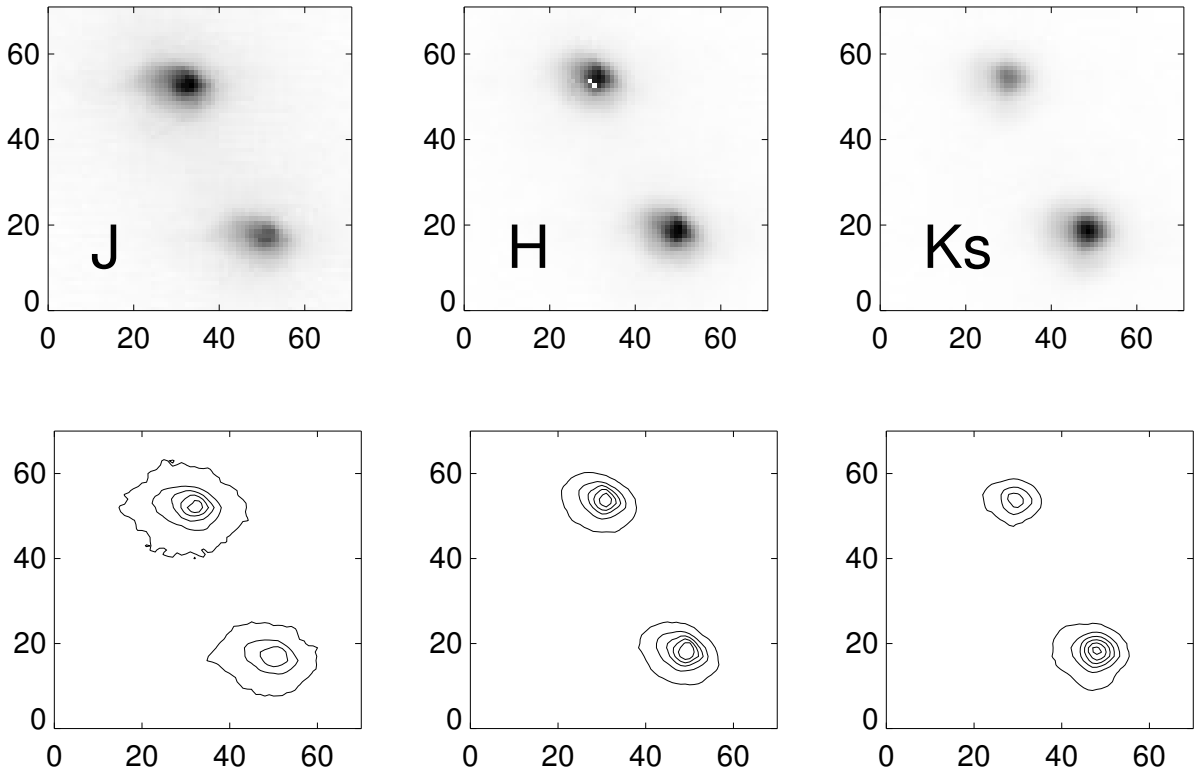

Fig. 1.— Keck LGS-AO NIRC2 images obtained on 15 April 2012. The J-band image is on the left, with H in the center and K_s on the right. The images are shown in the top row, with North up and East to the left. Contours of the objects, meant to more easily demonstrate the flux reversal, are shown in the bottom row. Axes indicate array coordinates (pixels); the NIRC2 narrow camera used for these observations has a pixel scale that is ≈10 mas pix^{-1} .

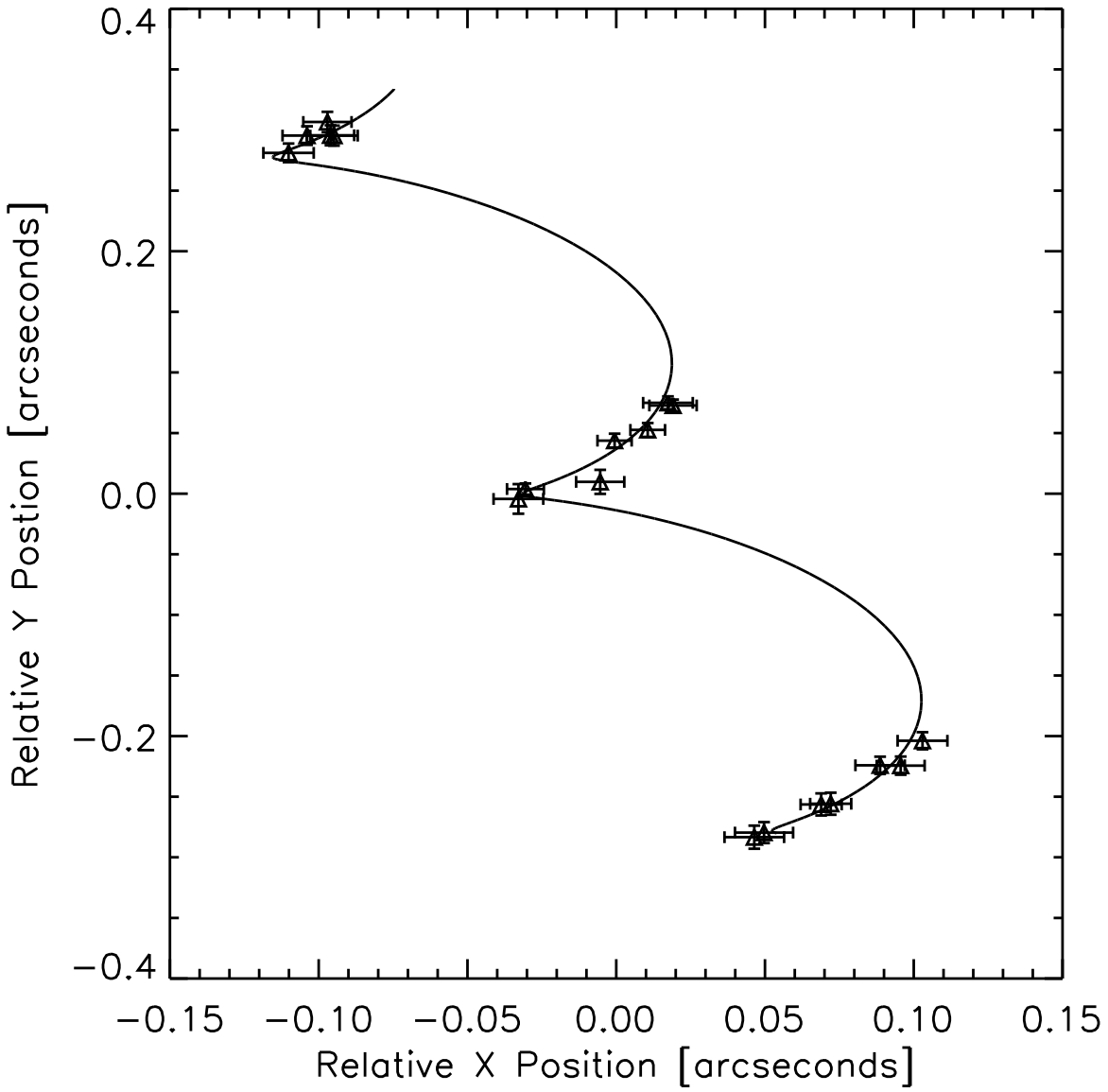

Fig. 2.— The apparent motion of WISE 0611−0410AB on the sky over twenty NTT epochs. The offsets are relative to the 10^{th} (?) observation. Also drawn is the best-fit parallactic curve through the data.

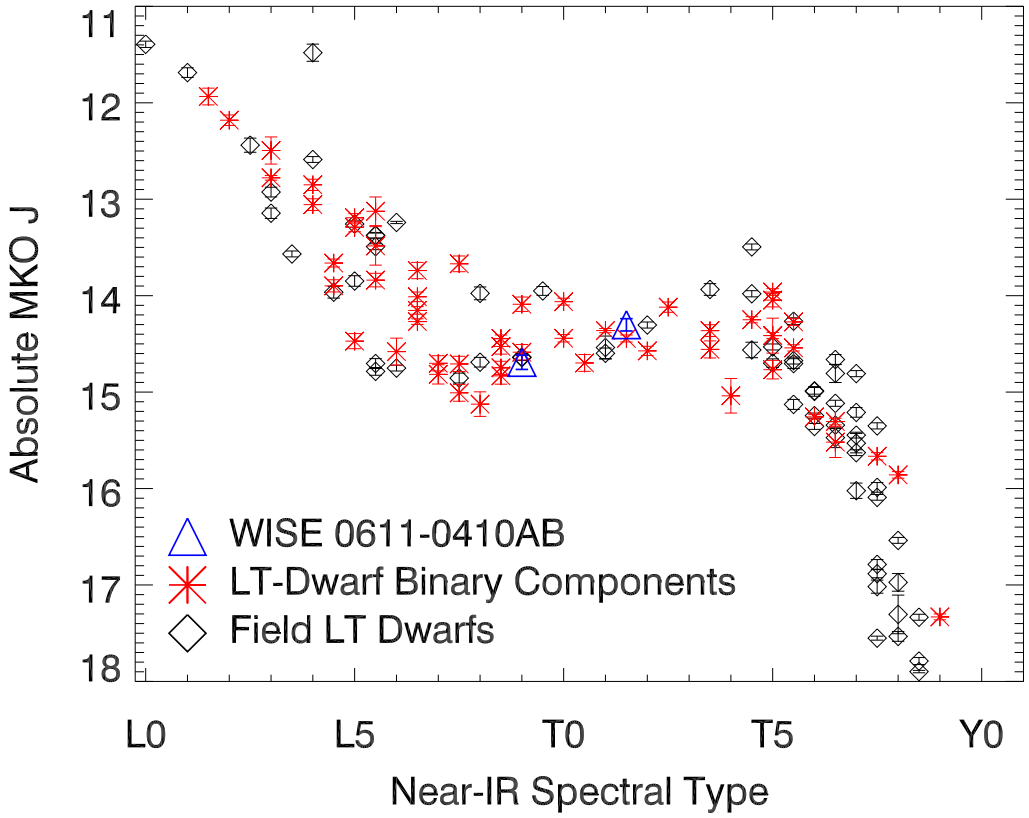

Fig. 3.— Absolute MKO J magnitude as a function of near-IR spectral type. Data from the other L and T dwarfs are taken from Dupuy & Liu (2012) and Burgasser et al. (2013), from which young and metal poor objects have been excluded. WISE 0611−0410 is denoted by the blue triangles, brown dwarf components in binary systems are denoted with red asterisks, and other brown dwarfs by the black diamonds.

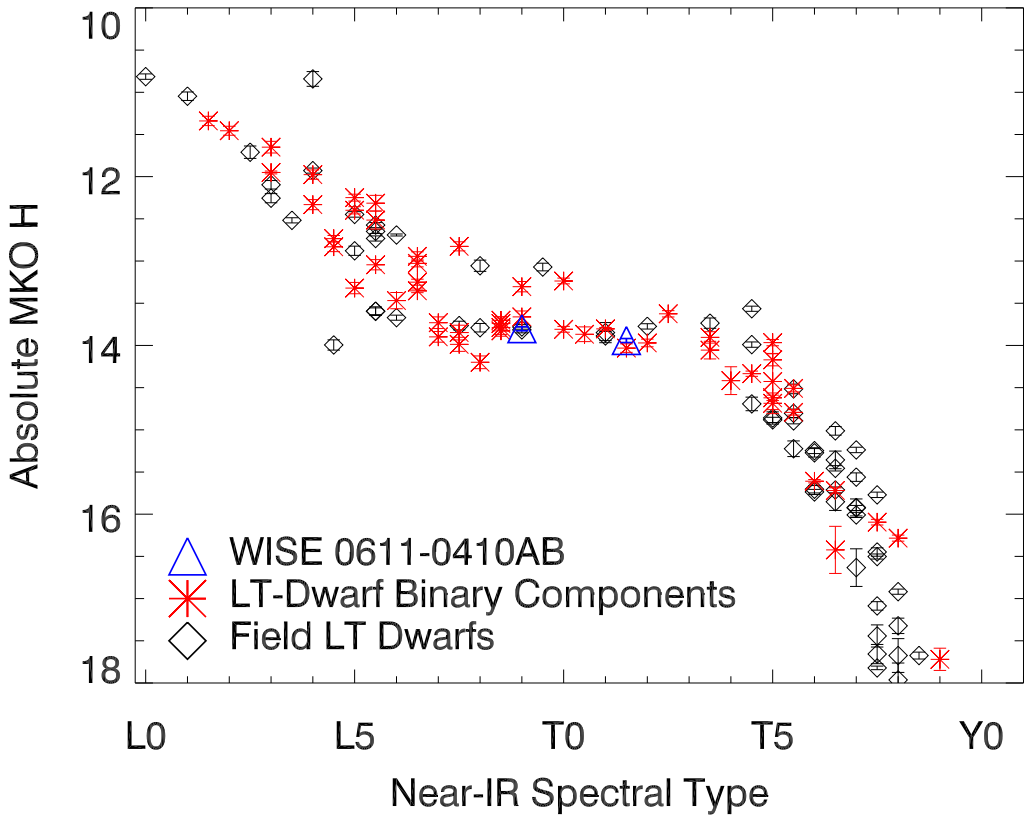

Fig. 4.— Absolute MKO H magnitude as a function of near-IR spectral type. Data and point types are the same as in Figure 3.

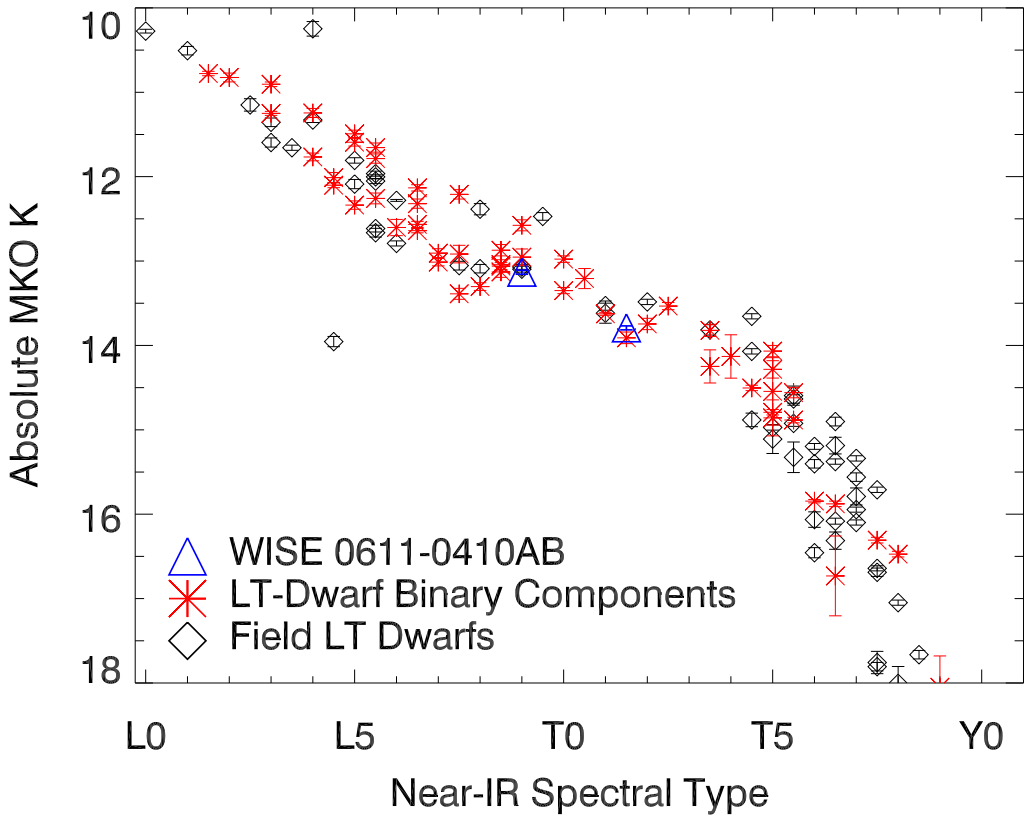

Fig. 5.— Absolute MKO K magnitude as a function of near-IR spectral type. Data and point types are the same as in Figure 3.

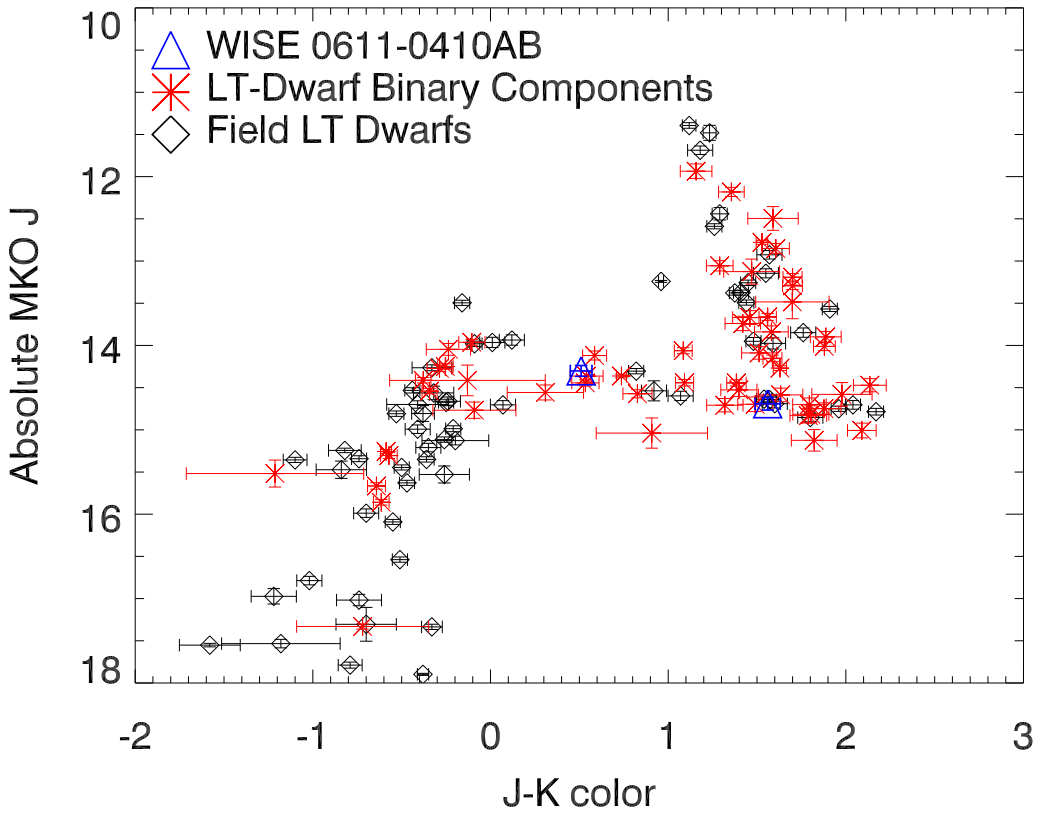

Fig. 6.— Absolute MKO J magnitude as a function of $J - K$ color. Data and point types are the same as in Figure 3.

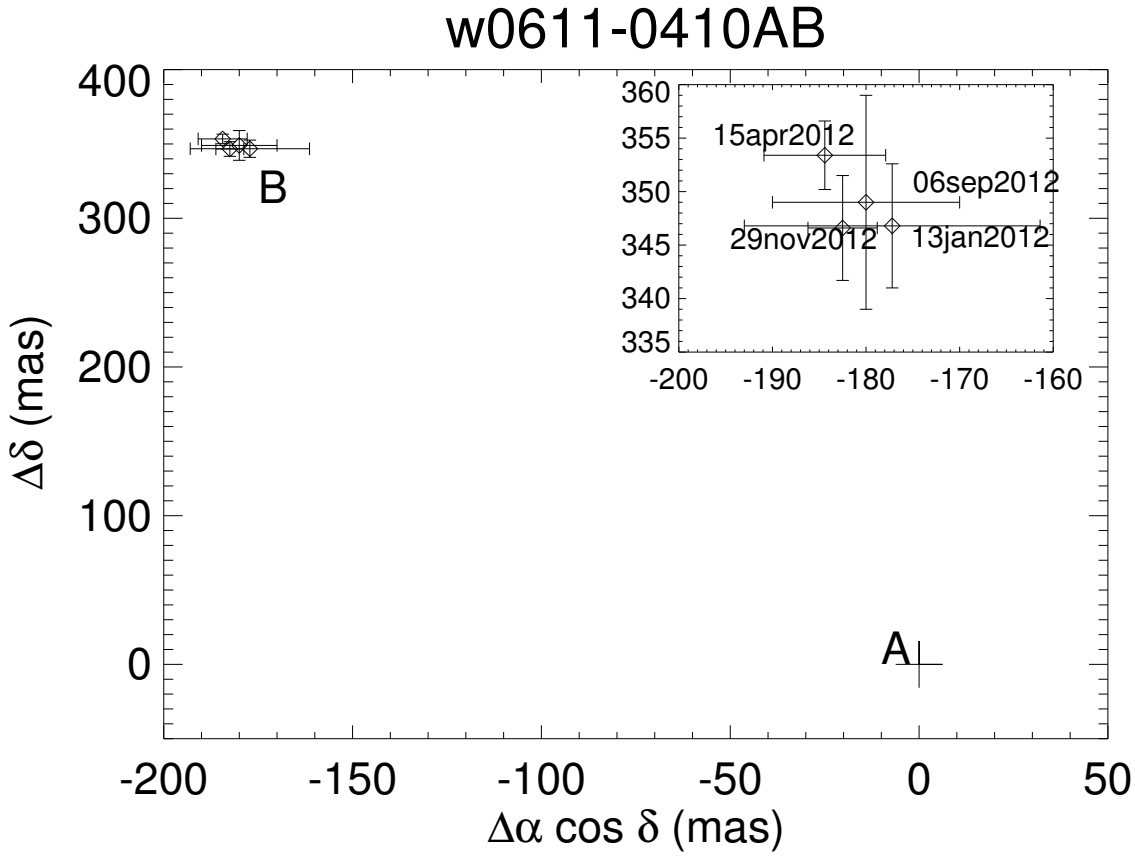

Fig. 7.— Motion of WISE 0611−0410B with respect to WISE 0611−0410A from NIRC2 data. The inset shows the four epochs in more detail. We do not detect any significant motion of the companion throughout our NIRC2 observations.

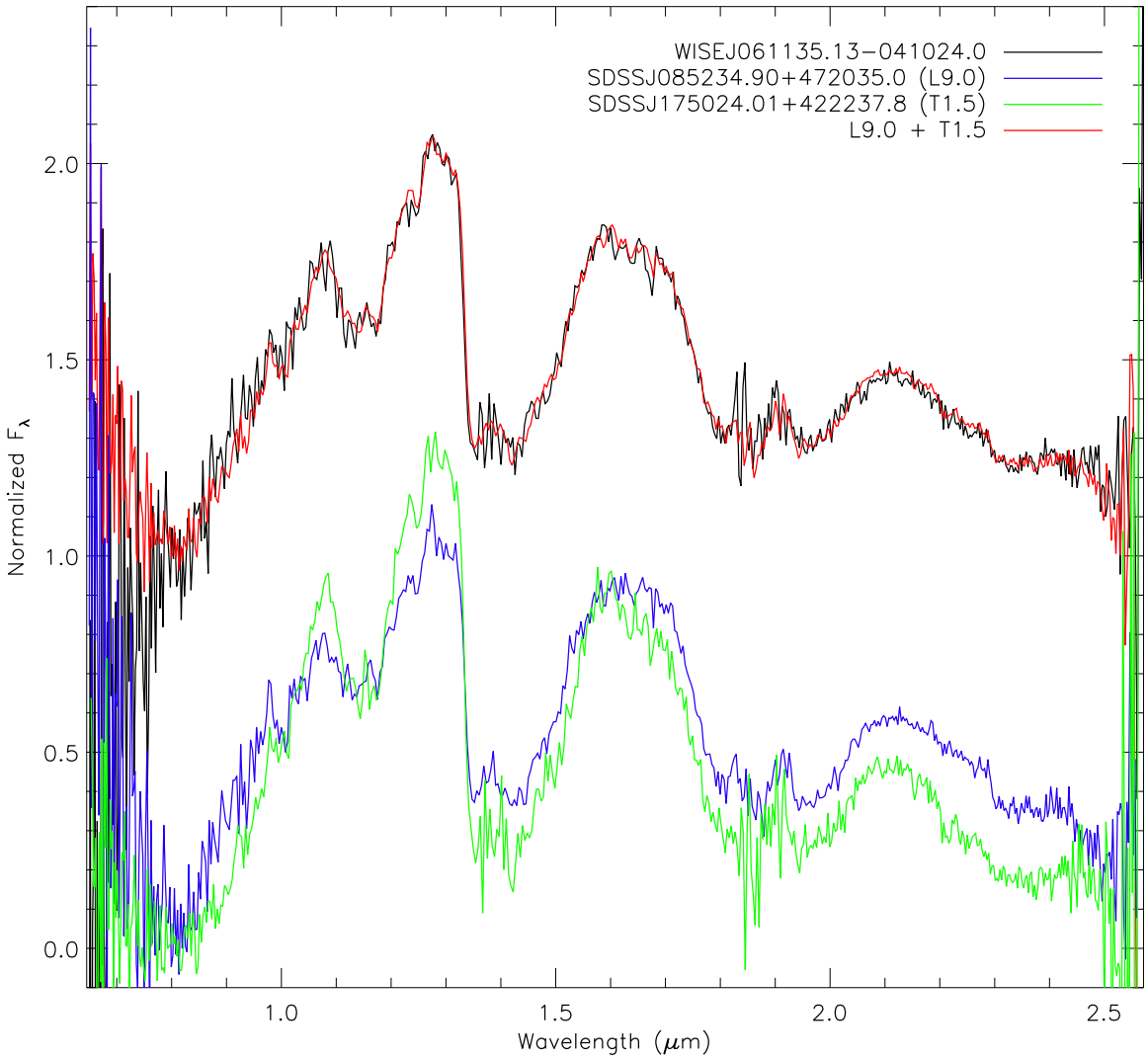

Fig. 8.— Near-IR spectra of WISE 0611−0410AB from Kirkpatrick et al. (2011, black (?) line). Also shown are the template L9 (SDSS J085234.90+472035.0; blue(?) line; REFERENCE) and T1.5 (SDSS J175024.01+422237.8; yellow(?) line; REFERENCE) spectra, whose convolution (red (?) line) provides the best fit to the observed WISEP J061135.13-041024.05AB spectrum. The spectra have been normalized at WHAT WAVELENGTH. The flux reversal between 1 and 1.3 μm observed in the NIRC2 photometry is also evident in the comparison of the template spectra.

Table 1. Flux Reversal Binaries

Binary	SpT_A	SpT_B	Discovery Method	Reference
2MASS J05185995−2828372AB	L6:	T4:	Spectral Decomp.	1
WISEP J061135.13-041024.05AB	L9	T1.5	LGSAO Imag., Spectral Decomp.	2
SDSS J102109.69−030420.1AB	T1	T4	Spectral Decomp.	1
WISE 104915.57−531906.1AB	L7.5	T0.5	Spectroscopy, Imag.	3
2MASS J14044941−3159329AB	T1±1	T5±1	LGSAO Imag.	4
SDSS J153417.05+161546.1AB	T1.5	T5.5	LGSAO Imag.	5
2MASS J17281150+3948593AB	L5	L6.5	HST Imag.	6, 7

References — (1) Burgasser et al. (2006); (2) this work; (3) Burgasser et al. (2013); (4) Looper et al. (2008); (5) Liu et al. (2006); (6) Gizis et al. (2003); (7) Burgasser et al. (2010)

Table 2. WISE 0611−0410 Photometry

Property	Value	Reference
Spectral Type (near-IR)	T0	3
$J_{\rm 2MASS}$	15.489±0.055	1
$H_{\rm 2MASS}$	14.645±0.048	1
$Ks_{\rm 2MASS}$	14.221±0.070	1
$J_{\rm MKO}$	15.32±0.06	2
$H_{\rm MKO}$	14.743±0.005	3
$K_{\rm MKO}$	14.292±0.005	3
IRAC 3.6 μm	13.069±0.017	4
IRAC 4.5 μm	12.924±0.017	4
WISE $W1$	13.566±0.027	5
WISE $W2$	12.933±0.032	5
WISE $W3$	>12.933	5
WISE $W4$	>9.075	5

References– (1)2MASS Catalog; (2)this work; (3)UKIDSS Catalog; (4) Kirkpatrick et al. 2011; (5) WISE Catalog

Table 3. NIRC2 Observing Log

Date [UT]	Filter	Exposure [sec]	Note
2012 Jan 13	H	1800	poor seeing
2012 Apr 15	J	180	good seeing
	H	180	good seeing
	Ks	180	good seeing
2012 Sep 06	H	30	only a single image obtained, but good seeing
2012 Nov 29	H	360	good seeing

Table 4. Parallax and Proper Motion

Parameter	Value
α, δ (J2000)	6:11:35.0, −4:10:24.9
Epoch [yr]	2013.1629
Absolute parallax [mas]	47.25 ± 3.22
μ_α [mas yr^{-1}]	83.7021 ± 2.50
μ_δ [mas yr^{-1}]	-279.13 ± 2.02
Relative to absolute correction [mas]	0.84
Duration of observations [yrs]	2.18
reference stars, no. of observations	19, 291

Table 5. Properties of WISE 0611−0410AB

Parameter	A	B	Δ
MKO J [mag]	16.23±0.07	15.93±0.06	−0.30±0.01
MKO H [mag]	15.43±0.01	15.57±0.01	0.14±0.01
MKO K [mag]	14.76±0.01	15.42±0.01	0.66±0.01
MKO $J-K$ [mag]	1.47±0.07	0.51±0.06	···
Est. Sp. Type	L9	T1.5	···

Table 6. NIRC2 Astrometry

	Measured		Predicted if BG object	
Date [UT]	$\Delta\alpha\cos(\delta)$ [mas]	$\Delta\delta$ [mas]	$\Delta\alpha\cos(\delta)$ [mas]	$\Delta\delta$ [mas]
2012 Jan 13	−177.2±15.8	346.8±5.8	−177.2	346.8
2012 Apr 15	−184.4±6.5	353.4±3.2	−205.7	424.3
2012 Sep 06	−180±10	349±10	−234.3	530.1
2012 Nov 29	−182.5±3.7	346.6±4.9	−256.1	591.9

Table 7. Mass and Period Predictions

Age [Gyr]	Mass A [$M_{\rm Jup}$]	Mass B [$M_{\rm Jup}$]	Orb. Period [yr]
0.5	30	26	147
1.0	42	37	124
3.0	72	63	94
5.0	92	81	83

REFERENCES

Burgasser, A. J., Geballe, T. R., Leggett, S. K., Kirkpatrick, J. D., & Golimowski, D. A. 2006, ApJ, 637, 1067

Burgasser, A. J., Marley, M. S., Ackerman, A. S., Saumon, D., Lodders, K., Dahn, C. C., Harris, H. C., & Kirkpatrick, J. D. 2002, ApJ, 571, L151

Burgasser, A. J., Sheppard, S. S., & Luhman, K. L. 2013, ArXiv e-prints

Burrows, A., Hubbard, W. B., Lunine, J. I., & Liebert, J. 2001, Reviews of Modern Physics, 73, 719

Burrows, A., Sudarsky, D., & Hubeny, I. 2006, ApJ, 640, 1063

Cox, A. N. 2000, Allen's Astrophysical Quantities, ed. A. N. Cox, 1

Day-Jones, A. C., et al. 2013, MNRAS, 430, 1171

Devillard, N. 1997, The Messenger, 87, 19

Dupuy, T. J., & Liu, M. C. 2012, ApJS, 201, 19

Fischer, D. A., & Marcy, G. W. 1992, ApJ, 396, 178

Kirkpatrick, J. D. 2005, ARA&A, 43, 195

Kirkpatrick, J. D., et al. 2010, ApJS, 190, 100

—. 2011, ApJS, 197, 19

—. 2012, ApJ, 753, 156

Knapp, G. R., et al. 2004, AJ, 127, 3553

Looper, D. L., Gelino, C. R., Burgasser, A. J., & Kirkpatrick, J. D. 2008, ApJ, 685, 1183

Marocco, F., et al. 2010, A&A, 524, A38

Mendez, R. A., & van Altena, W. F. 1996, AJ, 112, 655

Monet, D. G., et al. 2003, AJ, 125, 984

Moorwood, A., Cuby, J.-G., & Lidman, C. 1998, The Messenger, 91, 9

Mould, J. R. 1976, A&A, 48, 443

Mould, J. R., & Hyland, A. R. 1976, ApJ, 208, 399

Reid, I. N., & Hawley, S. L. 2000, New light on dark stars. Red dwarfs, low-mass stars, brown dwarfs.

Smart, R. L. e. a. 2013, MNRAS, submitted

Stephens, D. C., & Leggett, S. K. 2004, PASP, 116, 9

Tinney, C. G., Burgasser, A. J., & Kirkpatrick, J. D. 2003, AJ, 126, 975

Torres, G. 2010, AJ, 140, 1158

Tsuji, T., & Nakajima, T. 2003, ApJ, 585, L151

van Dam, M. A., et al. 2006, PASP, 118, 310

Wizinowich, P. L., et al. 2006, PASP, 118, 297

Wright, E. L., et al. 2010, AJ, 140, 1868